ACCSCIENCE PUBLISHING

International Journal of Bioprinting

RESEARCH ARTICLE

Three-dimensional bioprinted silk fibroin–hydroxypropyl cellulose scaffold loaded with tendon stem/progenitor cells for the prevention of heterotopic ossification following Achilles tendon injury

Xianzong Ning[1,2], Rui Du[1], Minghao Zhang[1], Yutao Yang[1], Fei Yu[1], Xiaoming Xu[2], Baoyuan Meng[2], and Kai Yan[1]*

[1]Division of Sports Medicine and Adult Reconstructive Surgery, Department of Orthopedic Surgery, Nanjing Drum Tower Hospital, Affiliated Hospital of Medical School, Nanjing University, Nanjing, Jiangsu, China

[2]Division of Sports Medicine and Joint Surgery, Department of Orthopedic Surgery, Nanjing Pukou People's Hospital, Liangjiang Hospital, Southeast University, Nanjing, Jiangsu, China

Abstract

Achilles tendon injury is a common musculoskeletal disorder, particularly prevalent among athletes and middle-aged/elderly populations. Heterotopic ossification (HO) following Achilles tendon injury is a frequent complication that significantly compromises patients' quality of life and athletic performance. Conventional conservative treatments and surgical interventions for HO often yield suboptimal outcomes, failing to restore native tendon functionality. Tissue engineering strategies integrating biomaterials and cells offer promising solutions for tendon regeneration and functional recovery. Three-dimensional bioprinting presents unique advantages in fabricating tissue-engineered scaffolds through precise control of architectural geometry and internal microstructure. In this study, we developed a novel silk fibroin (SF)–hydroxypropyl cellulose (HPC)–tendon stem/progenitor cell (TSPC) bioink with exceptional cytocompatibility and rheological properties. This bioink demonstrated superior printability for fabricating porous Achilles tendon scaffolds with high mechanical strength (elastic modulus: 85 MPa), controlled biodegradability, and optimal porosity (91%). *In vitro* experiments revealed that SF– HPC–TSPCs scaffolds promoted TSPC survival, migration, proliferation, and tenogenic differentiation within the scaffold microenvironment. *In vivo* assessments demonstrated that the scaffolds exhibited excellent biocompatibility, elicited no systemic inflammatory or immune responses, and effectively prevented HO in rat models of Achilles tendon injury. This study establishes a groundbreaking approach for addressing post-traumatic HO in tendon regeneration.

Keywords: Achilles tendon injury; Heterotopic ossification; Silk fibroin; Three-dimensional bioprinting; Tissue-engineered scaffold

***Corresponding author:**
Kai Yan (yank1214@163.com)

Citation: Ning X, Du R, Zhang M, *et al.* Three-dimensional bioprinted silk fibroin–hydroxypropyl cellulose scaffold loaded with tendon stem/progenitor cells for the prevention of heterotopic ossification following Achilles tendon injury. *Int J Bioprint.* 2025;11(4):297-314. doi: 10.36922/IJB025210203

Received: May 19, 2025
Revised: June 3, 2025
Accepted: June 17, 2025
Published online: June 17, 2025

1. Introduction

Achilles tendon injury commonly manifests as tendinopathy, particularly in athletes and middle-aged/elderly populations. The high incidence of this injury is primarily associated with intensive physical activity, overuse, and age-related degenerative changes.[1] Post-injury clinical manifestations typically include pain, swelling, and restricted mobility, significantly impairing patients' quality of life and athletic performance.[2]

Heterotopic ossification (HO) following Achilles tendon injury refers to the pathological formation of ectopic bone within tendon tissues or adjacent soft tissues and is a frequent complication. Research indicates that HO in tendons often occurs after severe trauma or surgical intervention. For instance, HO incidence rates reach 54% following distal biceps tendon repair,[3] and 52.1% of patients develop HO after severe radial head fractures.[4] Furthermore, the prevalence of HO in the Achilles tendon increases with age—potentially due to upregulated bone morphogenetic protein (BMP) expression in tendon stem/progenitor cells (TSPCs).[5] The pathological progression of HO involves endochondral ossification, encompassing three distinct phases: the inflammatory stage, chondrogenesis, and terminal osteogenesis.[6] Although the precise mechanisms remain incompletely elucidated, HO development is closely linked to inflammatory responses, aberrant activation of osteogenic signaling pathways, and alterations in mechanical stress.[7–10] Emerging evidence suggests that the inflammatory cascade and hypoxic microenvironment during the acute phase of tendon injury may potentiate HO initiation.[11] Crucially, the BMP signaling pathway has been identified as a pivotal regulator of ectopic bone formation.[12] Age-dependent upregulation of BMP expression in injured tendons enhances the osteogenic differentiation capacity of TSPCs, thereby accelerating HO pathogenesis.[5] Furthermore, alterations in mechanical loading—whether excessive or insufficient—have been implicated as HO triggers, as demonstrated by load-dependent osteogenic induction in a preclinical model.[10]

Currently, there is no unified standard for treating HO following Achilles tendon injury. Common clinical approaches include conservative and surgical therapies. Conservative treatments primarily involve pharmacological interventions, such as non-steroidal anti-inflammatory drugs to reduce inflammation and inhibit HO progression, as well as physical therapy to promote healing by improving local blood circulation and enhancing tendon flexibility. However, these approaches show limited efficacy, especially in advanced ossification stages.[13] Surgical treatments focus on removing HO bone tissue and reconstructing tendon architecture. While effective in restoring tendon function, surgical procedures carry risks of post-operative complications such as infection and reinjury.[14,15] Traditional therapeutic strategies often prove inadequate for restoring the original biomechanical function of the Achilles tendon.[16]

Recent advancements in tissue engineering have opened new avenues for tendon repair. By combining scaffolds, cells, and growth factors, tissue engineering facilitates tendon regeneration and functional recovery. The selection of biomaterials is pivotal in designing tissue-engineered scaffolds. An ideal scaffold must exhibit excellent biocompatibility and mechanical properties to support cell adhesion and proliferation while maintaining sufficient mechanical strength to endure physiological loads.[17] Additionally, the scaffold's microstructure should closely resemble native tissue architecture to direct cell alignment and tissue regeneration.[18]

Three-dimensional (3D) bioprinting demonstrates significant advantages in the fabrication of tissue-engineered scaffolds.[19,20] First, this technology allows precise control over scaffold geometry and internal microstructure, enabling the design of personalized and complex architectures.[20] Second, 3D bioprinting enables the simultaneous deposition of cells and biomaterials, creating cell-laden scaffolds with biological activity, which is critical for promoting tissue regeneration.[21] Additionally, the mechanical properties and biological functions of scaffolds can be optimized by modulating printing parameters such as nozzle pressure and layer thickness.[22,23] Bioink formulation is central to 3D bioprinting, primarily composed of biomaterials and seed cells. The selection of biomaterials remains an active research area, with current options broadly classified into synthetic polymers and natural biomaterials. Natural biomaterials have attracted extensive scientific interest due to their superior biocompatibility and low cytotoxicity.[24,25] Xu et al.[26] constructed a poly(lactide-co-glycolide) (PLGA)/type I collage biphasic scaffold using 3D bioprinting technology, which effectively promoted tendon repair and inhibited HO, achieving an 86% reduction in heterotopic bone volume. However, fragments released during collagen degradation can act as potent initiators, activating inflammatory mechanisms that may interfere with the tissue repair process.[27] Moreover, the acidic degradation products of PLGA may alter the local pH, thereby inducing inflammatory responses and compromising biocompatibility.[28]

Silk fibroin (SF), a natural biomaterial, has attracted considerable interest due to its exceptional biocompatibility and tunable biodegradability.[29–31] In its native state, SF predominantly adopts a random coil conformation.[32] However, chemical modifications in hydroxyl-rich

environments can induce structural reorganization into ordered β-sheet configurations.[33] This conformational transition not only enhances SF's mechanical properties but also expands its biomedical applicability.[34] Hydroxypropyl cellulose (HPC), another biomaterial characterized by an abundance of hydroxyl groups, has been widely employed to optimize SF performance. The incorporation of HPC facilitates SF's structural transition from random coils to β-sheets, thereby improving mechanical robustness and structural stability.[35] Notably, HPC-mediated molecular interactions induce the formation of dual-network hydrogels through this conformational shift, resulting in superior mechanical strength and elasticity.[36] These SF–HPC composite hydrogels demonstrate significant potential for biomedical applications, particularly in leveraging their synergistic biocompatibility and controlled degradation profiles.

TSPCs, first identified in 2007,[37] are multi-potent cells capable of differentiating into tenocytes, chondrocytes, and osteoblasts, playing a pivotal role in tendon repair.[38] TSPCs address this challenge by undergoing tenogenic differentiation to promote collagen synthesis and extracellular matrix deposition, thereby facilitating functional tissue regeneration.[39] Furthermore, TSPCs enhance tendon healing through immunomodulatory effects, stimulation of tenocyte proliferation, and acceleration of collagen remodeling.[40] In tissue engineering, TSPCs are frequently integrated with biomaterial scaffolds to orchestrate neo-tendon formation. The combination of TSPCs with biocompatible scaffolds provides a biomimetic microenvironment that supports cell adhesion, migration, proliferation, and lineage-specific differentiation. For instance, decellularized tendon scaffolds functionalized with collagen have demonstrated efficacy in promoting TSPC proliferation and tenogenic commitment, ultimately enhancing the functional regeneration of damaged tendons.[40] This synergistic approach exhibits substantial potential for advancing tendon tissue engineering applications.

In summary, this study pioneers the development of a novel SF–HPC–TSPC bioink, formulated with SF as the matrix, HPC as a reinforcing agent, and TSPCs as the cellular component. We first characterized the rheological properties of this bioink and subsequently employed it for 3D bioprinting of tissue-engineered Achilles tendon scaffolds. The printed scaffolds were rigorously evaluated for mechanical properties, degradation behavior, and porous microstructure. *In vitro* investigations systematically assessed the scaffold's ability to regulate TSPC survival, migration, proliferation, and tenogenic differentiation. Furthermore, *in vivo* studies validated the scaffold's efficacy in preventing HO following Achilles tendon injury while concurrently evaluating systemic inflammatory and immune responses.

2. Materials and methods

2.1. Formulation of bioink

A total of 1.0 g SF, 1.0 g HPC, and TSPCs at a density of 5×10^6 cells/mL were added to 10 mL phosphate-buffered saline (PBS). The mixture was gently homogenized using a magnetic stir bar at 100 rpm for 10 min to avoid cellular damage. To identify the optimal bioink composition, cross-combinations of SF (0.5 g, 1.0 g, 1.5 g) and HPC (1.5 g, 1.0 g, 0.5 g) were systematically tested. The 1:1 SF–HPC ratio (1.0 g SF + 1.0 g HPC) demonstrated superior rheological properties and was selected for subsequent experiments. For the SF control bioink, 2.0 g SF and TSPCs (5×10^6 cells/mL) were dissolved in 10 mL PBS under identical mixing conditions. During the experimental process, we observed that the viscosity of the SF–HPC bioink was proportional to the concentration of HPC. However, when bioink with an SF–HPC ratio of 1.5:0.5 was used for 3D printing, the viscosity was too low to prevent scaffold collapse. Conversely, bioink with an SF–HPC ratio of 0.5:1.5 tended to cause nozzle clogging during 3D printing. Therefore, a 1:1 SF–HPC ratio was determined to be the optimal formulation. TSPCs (No. CP-R165) used in the experiments were purchased from Procell Life Science & Technology Co., Ltd (China). Experiments were conducted using cells at passages 2–3, as this stage is considered optimal for maintaining cellular functionality.

2.2. Rheological characterization of bioink

The rheological properties of the bioinks were analyzed using a modular advanced rheometer system (Thermo, USA). Dynamic viscosity was measured under shear rate sweeps from 0.1 to 100 s^{-1} at 37°C. Frequency-dependent storage modulus (G') and loss modulus (G") were determined through dynamic frequency sweep tests conducted over 30 min at 37°C.

2.3. Three-dimensional bioprinting of tissue-engineered Achilles tendon scaffolds

The SF–HPC–TSPCs bioink formulated in **Section 2.1** was employed to fabricate tissue-engineered Achilles tendon scaffolds using a multi-nozzle 3D bioprinter (Discovery, Switzerland). A computer-aided design model of the scaffold structure was first created, followed by loading the bioink into the pressure-assisted nozzle cartridge of the bioprinter. Printing parameters were set to a nozzle pressure of 0.25 mPa and a deposition speed of 1.0 mm/s. Scaffolds with final dimensions of 2 × 3 × 15 mm (width × height × length) were bioprinted onto sterile petri dishes under controlled environmental conditions (25°C; 60% relative humidity).

2.4. Mechanical testing of tissue-engineered Achilles tendon scaffolds

Scaffolds were centrally positioned on a testing fixture and subjected to uniaxial tensile loading at a constant rate of 1.0 mm/min using a universal mechanical testing machine (Instron, USA). Pressure was applied until scaffold rupture occurred, with mechanical parameters (stress, strain) automatically recorded. Elastic modulus was calculated from the linear elastic region of the stress-strain curves. Additionally, cyclic tensile testing was performed on both SF and SF–HPC scaffolds. Data visualization and analysis were performed using GraphPad Prism 9.0 (GraphPad, USA) and Origin Pro 2023 software (Origin Lab, USA).

2.5. Degradation assessment of scaffolds

For *in vitro* degradation, scaffolds were incubated in PBS containing 0.1 U/mL proteinase XIV or enzyme-free PBS at 37°C. Specimens were retrieved on days 0, 2, 4, 8, and 16, followed by gravimetric analysis to calculate degradation rates. For *in vivo* degradation, scaffolds were subcutaneously implanted into nude mice (BALB/c-nu; male' 6 weeks old; obtained from Weitong Lihua Limited Company (China); n = 24) under sodium pentobarbital anesthesia (50 mg/kg, intramuscular). Animals were sacrificed at predetermined intervals (0, 2, 4, 8, and 16 days) for scaffold retrieval and degradation rate calculation using the same gravimetric protocol.

2.6. Scanning electron microscopy analysis of scaffold microarchitecture

Scaffolds were imaged using a scanning electron microscope (SEM; Hitachi, Japan). Prior to imaging, scaffolds were pre-cooled at −20°C for 4 h, transferred to −80°C for 15 min, and lyophilized in a pre-chilled freeze dryer for 12 h. Specimens were sectioned, mounted on SEM stubs, and sputter-coated with 10 nm gold/palladium (Quorum, UK) to enhance conductivity. Microstructural images were acquired at an accelerating voltage of 5 kV. Porosity and pore size distribution were quantified from SEM images using ImageJ (NIH, USA).

2.7. Live/dead cell staining

TSPC-seeded scaffolds were cultured for 72 h in Dulbecco's modified eagle medium/nutrient mixture F12 medium supplemented with 10% fetal bovine serum. Cells were stained using a viability/cytotoxicity kit (Thermo, USA) containing 4 μM calcein-acetoxymethyl (live cells; green) and 2 μM ethidium homodimer-1 (EthD-1; dead cells; red) for 30 min at 37°C. Fluorescent images were captured with a confocal microscope (Leica, Germany) at 488 nm/530 nm (calcein) and 552 nm/617 nm (EthD-1) excitation/emission. Cell viability was calculated as (live cells/total cells) × 100 using ImageJ with the Cell Counter plugin.

2.8. Transwell migration assay

To evaluate the migratory capacity of TSPCs in SF and SF–HPC scaffolds, a Transwell migration assay was conducted. SF and SF–HPC scaffolds containing 1×10^5 cells were placed in the upper chamber of Transwell inserts (Corning, USA) with serum-free medium. The lower chamber was filled with 500 μL complete medium containing 10% fetal bovine serum. After 36 h incubation, scaffolds were removed, and non-migrated cells on the upper membrane surface were carefully wiped off. Migrated cells on the lower membrane were fixed with 4% paraformaldehyde and stained with 0.5% crystal violet. Three random fields per insert were imaged under an inverted microscope (Nikon, Japan), and migrated cells were quantified using ImageJ with the Cell Counter plugin.

2.9. Scratch wound healing assay

TSPCs were harvested from SF and SF–HPC scaffolds and seeded into six-well plates until 80–90% confluency. A uniform scratch wound was created using a sterile 200 μL pipette tip. Wound closure was monitored at 0, 12, 24, and 36 h under phase-contrast microscopy (Leica, Germany). Wound width was measured at three predefined positions per well using ImageJ.

2.10. Cell Counting Kit-8 proliferation assay

TSPCs (1×10^3 cells/well), harvested from scaffolds, were seeded into 96-well plates (Corning, US) in triplicate. Cell proliferation was assessed at 12, 24, and 72 h using a Cell Counting Kit-8 (CCK-8; Dojindo, Japan). After 4 h of incubation with CCK-8 reagent at 37°C, absorbance at 450 nm was measured using a microplate reader (Thermo, USA).

2.11. Quantitative reverse transcription polymerase chain reaction

TSPC-laden scaffolds were cultured for 2 and 4 weeks. Total RNA was extracted using TRIzol reagent (Thermo, USA) following scaffold homogenization. After centrifugation (10,000 rpm; 10 min; 4°C), RNA was reverse-transcribed into cDNA using the SuperScript IV First-Strand Synthesis System (Thermo, USA). Quantitative reverse transcription polymerase chain reaction (PCR) was performed on a QuantStudio 5 System (Thermo, USA) using PowerUp SYBR Green Master Mix. Gene expression of tenogenic (scleraxis [*Scx*]), chondrogenic (SRY-box transcription factor 9 [*Sox9*]), and osteogenic (bone morphogenetic protein 2 [*Bmp2*]) markers was normalized to glyceraldehyde 3-phosphate dehydrogenase.

2.12. Achilles tendon transection repair and scaffold implantation in rats

Male Sprague–Dawley rats (**aged 4–6 weeks;** obtained from Weitong Lihua Limited Company (China); n = 36)

were anesthetized with 3% sodium pentobarbital (0.8 mL/kg; intravenous). The skin and subcutaneous tissue of the hind paw heel were incised layer by layer to expose the Achilles tendon, which was then transected at its midportion using a scalpel. In the control group, the severed tendons were repaired directly with 4-0 absorbable sutures using a modified Kessler technique. The subcutaneous tissue and skin were subsequently closed in layers with 3-0 absorbable sutures. In the scaffold group, appropriately sized scaffolds were sutured to the tendon stumps with 4-0 absorbable sutures prior to the layered closure of subcutaneous tissue and skin with 3-0 absorbable sutures. This animal experiment was approved by the Ethics Committee of Drum Tower Hospital, School of Medicine, Nanjing University (No. 2021AE01031).

2.13. Micro-computed tomography imaging for heterotopic ossification quantification

Micro-computed tomography (CT) scanning (Skyscan, Belgium) was performed on control, SF, and SF–HPC groups at 2, 4, and 8 weeks post-Achilles tendon transection to quantify HO volume. Scan parameters included a 65 kV source voltage, 300 μA current, and 18 μm isotropic voxel size. Raw data were reconstructed using Mimics Research 20.0 (Materialise, Belgium), and HO volumes were segmented and calculated in Magics 25.0 (Materialise, Belgium) using a fixed Hounsfield unit threshold (800–3000).

2.14. Histological analysis

Tendon specimens harvested at 8 weeks were fixed in 4% paraformaldehyde for 72 h, decalcified in 15% EDTA with daily solution renewal, and paraffin-embedded. Sections (5 μm thick) were stained as follows: hematoxylin and eosin (H&E) for general tissue morphology; Safranin O for proteoglycan/cartilage matrix visualization; and BMP-2 immunohistochemistry (IHC) using an anti-BMP-2 primary antibody (ab214821; Abcam, UK) and 3,3'-diaminobenzidine chromogen.

2.15. Hematological profiling

Systemic inflammatory and immune responses were assessed via complete blood count analysis (Sysmex, Japan) at days 3, 7, and 14 post-implantation. Key parameters included: leukocyte count (white blood cell [WBC]; $\times 10^9$/L), erythrocyte count (red blood cell; $\times 10^{12}$/L), neutrophil count ($\times 10^9$/L), neutrophil percentage, lymphocyte count ($\times 10^9$/L), lymphocyte percentage, monocyte count ($\times 10^9$/L), monocyte percentage, interleukin-6 concentration (IL-6), and tumor necrosis factor-α concentration (TNF-α).

2.16. Statistical analysis

All data are expressed as mean ± standard deviation. Intergroup comparisons were analyzed using a one-way analysis of variance with Tukey's post-hoc test (for ≥3 groups) or unpaired Student's *t*-test (for two groups) using GraphPad Prism 9.0. Significance thresholds were defined as: $^*p < 0.05$, $^{**}p < 0.01$, $^{***}p < 0.001$, $^{****}p < 0.0001$.

3. Results and discussion

3.1. Rheological properties of bioinks

To evaluate the rheological properties of SF and SF–HPC bioinks, steady-state shear tests and dynamic oscillatory tests were performed. The shear rate–viscosity curve (Figure 1A) demonstrated that the viscosities of both SF

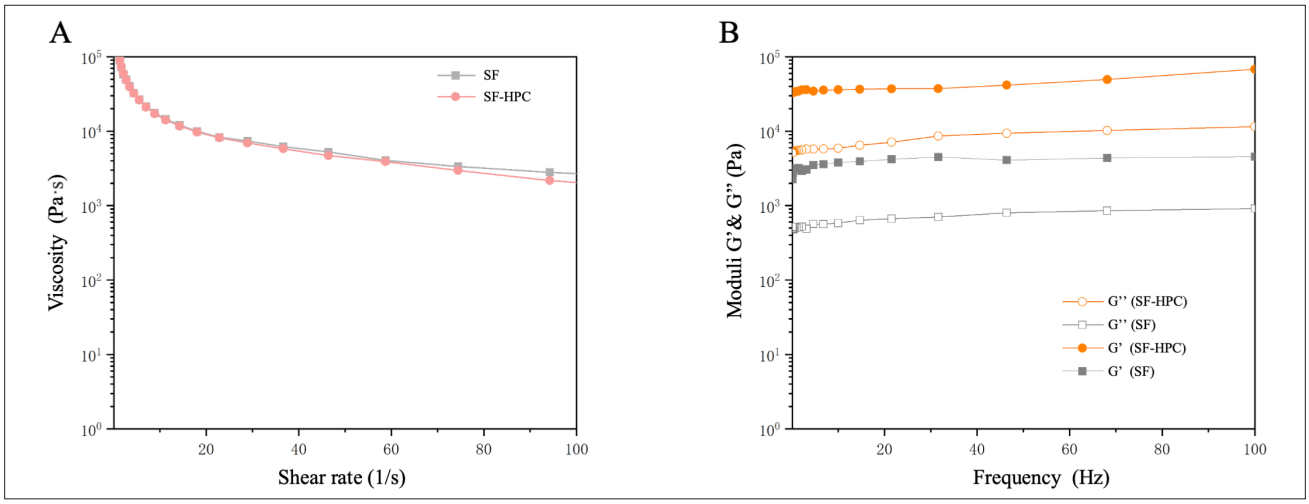

Figure 1. Rheological characterization of SF and SF–HPC bioinks. (A) Shear rate-dependent viscosity curves. (B) Frequency-dependent storage modulus (G') and loss modulus (G"). Abbreviations: HPC, hydroxypropyl cellulose; SF, silk fibroin.

and SF–HPC bioinks gradually decreased with increasing shear rate, indicating favorable shear-thinning behavior. Shear-thinning capability is one of the core requirements for extrusion-based 3D bioprinting.[41] At the high shear rate near the printer nozzle, viscosity decreased significantly, enabling the bioinks to pass through the micro-nozzle with low resistance, thereby preventing nozzle clogging due to high viscosity. Upon exiting the nozzle, the shear rate abruptly dropped, and viscosity rapidly recovered, enhancing scaffold shape stability and preventing structural collapse or deformation. Equally important, when using cell-laden bioinks for 3D printing, shear-thinning properties enable smooth extrusion under lower printing pressure, reducing cell membranes or extracellular matrix damage caused by high shear stress and improving cell viability.[42] Following extrusion, rapid viscosity recovery immobilizes cells, preventing gravity or flow-induced migration during the molding stage and ensuring uniform cell distribution within the printed structure.

The frequency–modulus curve (Figure 1B) showed that the G' and G" of both SF and SF–HPC bioinks remained relatively stable with increasing frequency. Notably, the G' of both bioinks exceeded their respective G", indicating that both formulations exhibited stable gel-like behavior. Furthermore, the G' of SF–HPC bioinks was higher than that of SF bioinks, suggesting that the incorporation of HPC into SF enhanced cross-linking and promoted a more stable network within the bioink. In conclusion, excellent rheological properties are crucial for successful extrusion-based 3D bioprinting, as they directly affect the bioinks' extrusion controllability, structural fidelity, cell viability, and ultimately the functionality of engineered tissues.[43]

3.2. Three-dimensional bioprinting of tissue-engineered Achilles tendon scaffolds and bending tests

Extrusion-based 3D bioprinting was employed to fabricate tissue-engineered Achilles tendon scaffolds with dimensions of 2 mm × 3 mm × 15 mm (Figure 2A–C). During the printing process, the bioink extruded smoothly from the nozzle without clogging. The printed scaffolds maintained structural integrity with no observable deformation or collapse, demonstrating excellent printing fidelity. Bending tests revealed that the scaffolds could be bent to 180° without fracture and fully recovered to their original shape after unloading (Figure 2D1–D3). SF–HPC scaffolds showed no fracture during bending, indicating superior toughness and ductility. Complete shape recovery after bending further confirmed their appropriate elastic modulus. Previous studies have demonstrated that scaffold toughness, ductility, and elastic modulus are critical factors for tendon injury repair.[44] Specifically, the Achilles tendon undergoes significant tension during physical activities

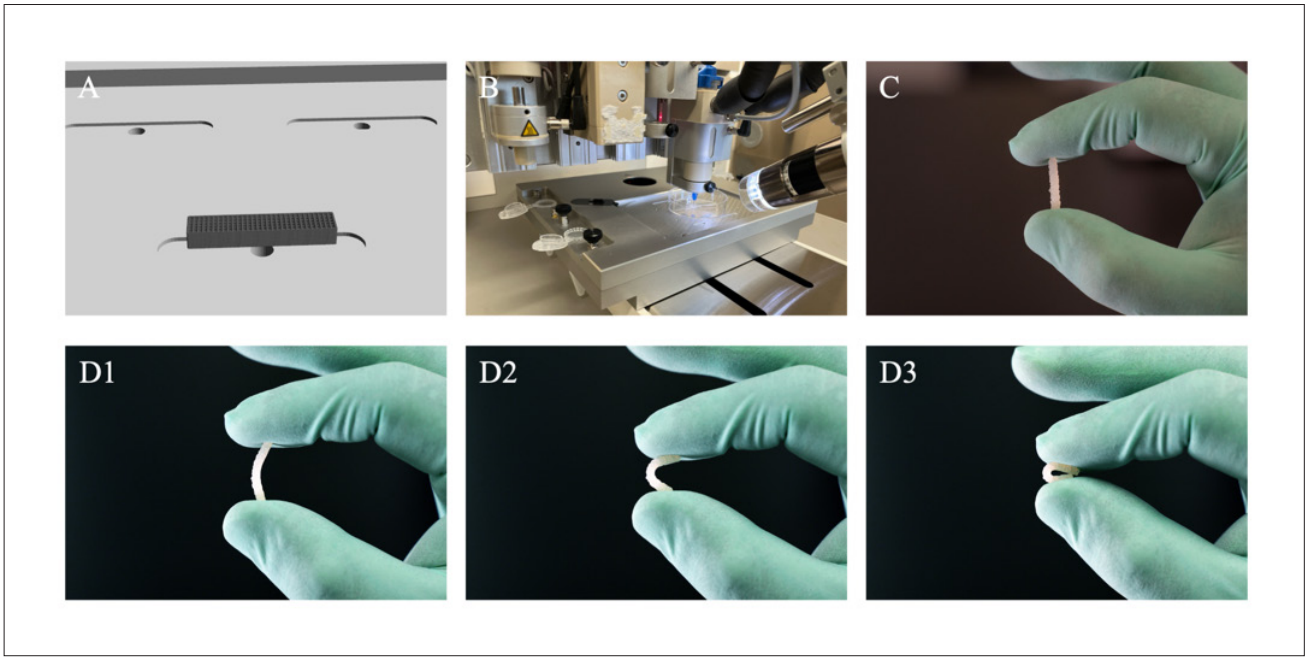

Figure 2. Fabrication and bending test of 3D bioprinted tissue-engineered Achilles tendon scaffolds. (A) Digital design model prior to bioprinting. (B) 3D bioprinting process. (C) Macroscopic view of the printed scaffold. (D1–D3) Sequential bending test demonstrating elastic recovery (180° bending angle) and preserved structural integrity (no fractures observed). Abbreviation: 3D, three-dimensional.

and must deform to accommodate mechanical loads. Our findings suggest that the SF–HPC scaffolds possess optimal toughness, ductility, and elastic modulus to withstand the tensile forces required for functional Achilles tendon repair.

3.3. Elastic modulus and degradation properties of tissue-engineered Achilles tendon scaffolds

In the design of tissue-engineered Achilles tendon scaffolds, elastic modulus is a critical determinant of scaffold functionality and biocompatibility.[45] The scaffold's elastic modulus must closely match that of the native Achilles tendon to avoid stress-shielding effects.[46,47] An excessively high elastic modulus may cause the scaffold to bear the majority of mechanical loads, thereby reducing mechanical stimulation to surrounding native tissue and impairing regeneration. Conversely, an insufficient elastic modulus could compromise structural support, leading to deformation or fracture and a failure to transmit mechanical signals effectively. In this study, the elastic modulus of SF–HPC scaffolds was measured at 85 MPa, significantly higher than that of pure SF scaffolds (55 MPa) (Figure 3A and B). Notably, the elastic modulus of SF–HPC scaffolds approached values comparable to native Achilles tendon tissue. Additionally, cyclic tensile testing was performed on both SF and SF–HPC scaffolds. The results demonstrated that, compared to SF scaffolds, SF–HPC scaffolds maintained a well-preserved elastic modulus after multiple cycles of tensile loading, indicating favorable resistance to stress fatigue (Figure 3C and D).

Tissue-engineered scaffolds are typically biodegradable and gradually absorbed during neo-tissue formation.[48] The degradation rate must be synchronized with the development of mechanical properties in the regenerating tissue to ensure a stable mechanical environment throughout the healing process.[49] Degradation tests demonstrated that both SF and SF–HPC scaffolds underwent degradation in PBS solution, protease XIV solution, and *in vivo* conditions (Figure 3E–G). Notably, SF–HPC scaffolds exhibited more stable degradation rates that closely matched the remodeling kinetics of tendon tissue.

This study identified the elastic modulus of the 3D-bioprinted tissue-engineered tendon scaffold as the primary contributor to enhanced tendon repair. The scaffolds' modulus was engineered to match the biomechanical properties of the injured tendon, thereby providing sufficient mechanical support during healing while preventing secondary damage from excessive

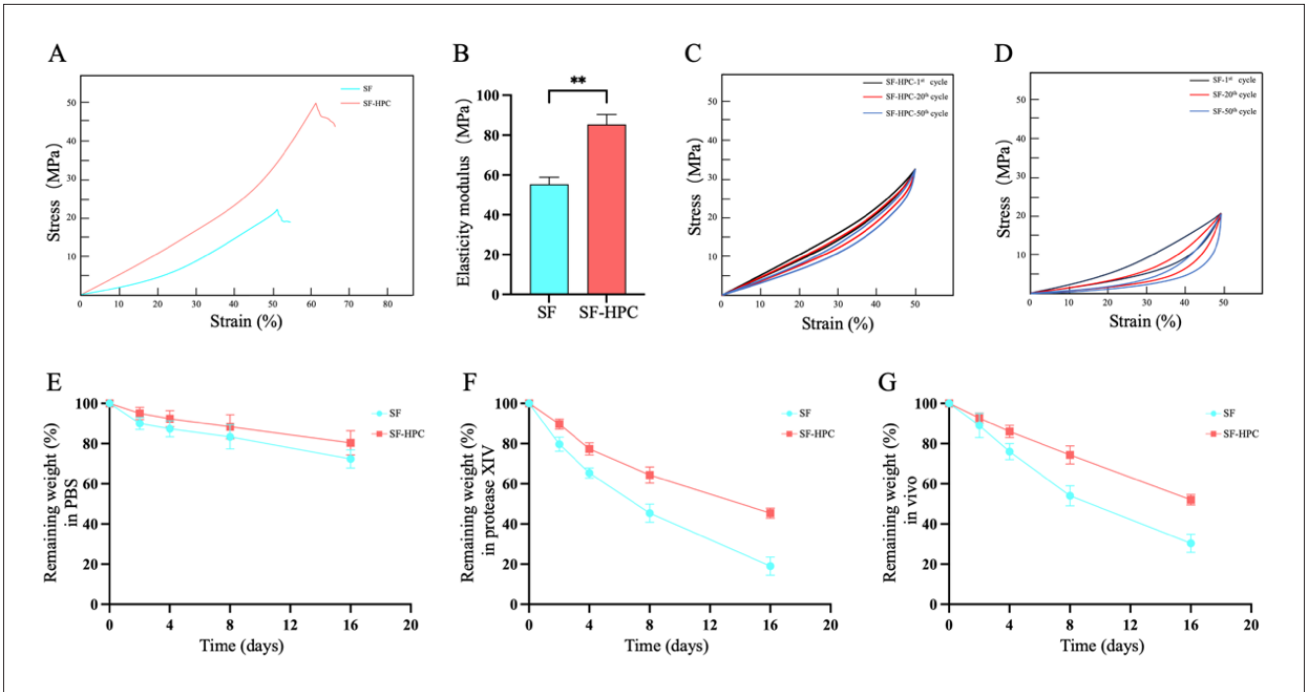

Figure 3. Mechanical and degradation properties of SF and SF–HPC tissue-engineered Achilles tendon scaffolds. (A) Stress–strain curves. (B) Elastic modulus. (C) Cyclic tensile testing of SF–HPC scaffolds. (D) Cyclic tensile testing of SF scaffolds. (E) *In vitro* degradation in PBS. (F) Enzymatic degradation in protease XIV solution. (G) *In vivo* degradation profile. $n = 3$; $^{**}p < 0.01$. Abbreviations: HPC, hydroxypropyl cellulose; SF, silk fibroin; PBs, phosphate-buffered saline.

stress concentration. Furthermore, as supported by prior research, an optimal elastic modulus maintains physiological tendon function and significantly enhances the proliferation of tendon-derived cells on the scaffolds, ultimately facilitating superior tendon regeneration.[50]

3.4. Pore structure analysis of tissue-engineered Achilles tendon scaffolds

To analyze the pore structure of tissue-engineered Achilles tendon scaffolds, SEM was performed on both SF and SF–HPC scaffolds. The SEM results revealed that SF–HPC scaffolds exhibited a more uniform pore distribution compared to SF scaffolds (Figure 4A1, A2, B1, and B2). The pore size of SF–HPC scaffolds predominantly ranged between 50–150 μm, whereas SF scaffolds showed pore sizes primarily distributed within 0–50 μm (Figure 4D). Furthermore, SF–HPC scaffolds demonstrated a porosity of 91%, significantly higher than the 78% porosity observed in SF scaffolds (Figure 4C). The porous architecture, porosity, and pore size of tissue-engineered scaffolds are critical determinants of their biofunctionality, as these parameters directly regulate cell migration, proliferation, differentiation, and nutrient transport.[51] The interconnected porous structure provides a 3D growth space for cells, facilitating adhesion, proliferation, and migration.[52] High porosity enhances cell infiltration and nutrient diffusion, thereby promoting cellular activities within the scaffold.[53]

3.5. Cell viability, migration, proliferation, and differentiation in tissue-engineered Achilles tendon scaffolds

To evaluate cell viability within the scaffolds, a live/dead cell staining assay was performed on SF and SF–HPC scaffolds. The results demonstrated that SF–HPC scaffolds exhibited 92% cell viability, significantly higher than the 85% viability observed in SF scaffolds (Figure 5A–C). The superior viability in SF–HPC scaffolds indicates the non-cytotoxic nature of the scaffold material and the absence of cellular damage from degradation products. Furthermore, the interconnected porous architecture facilitated nutrient exchange, which contributed to enhanced cellular survival.[54]

To assess cell migration capacity within the scaffolds, Transwell assays and scratch wound assays were conducted. The Transwell assay showed that the SF–HPC group exhibited an average of 115 migrated cells per microscopic field, significantly higher than the 85 cells observed in the SF group (Figure 5D–F). Scratch assay results revealed a gradual narrowing of the scratch gap over time in both

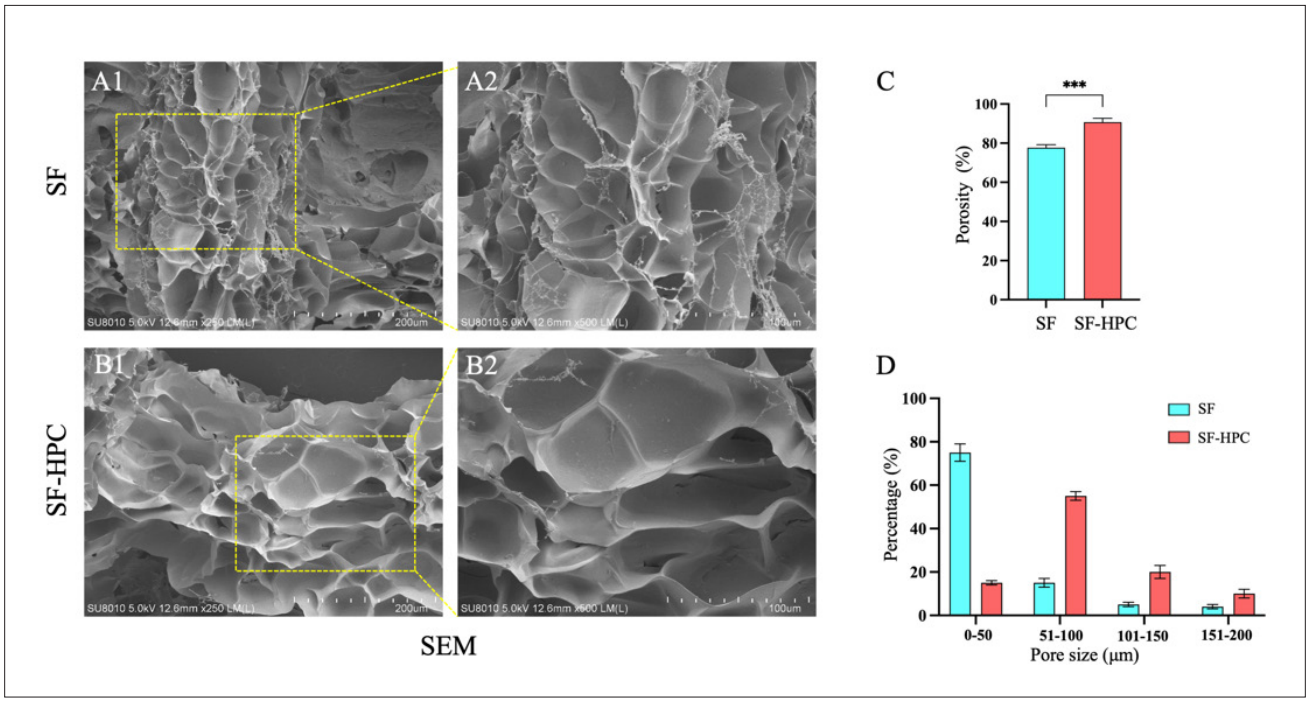

Figure 4. SEM characterization, porosity, and pore size distribution of SF and SF–HPC tissue-engineered Achilles tendon scaffolds. (A1, A2) Representative SEM images of SF scaffolds. (B1, B2) Representative SEM images of SF–HPC scaffolds. Scale bars: (A1, B1) 200 μm, (A2, B2) 100 μm; magnification: (A1, B1) 250×, (A2, B2) 500×. (C) Porosity comparison between SF and SF–HPC scaffolds. (D) Pore size distribution of SF and SF–HPC scaffolds. $n = 3$; ***$p < 0.001$. Abbreviations: HPC, hydroxypropyl cellulose; SF, silk fibroin; SEM, scanning electron microscopy.

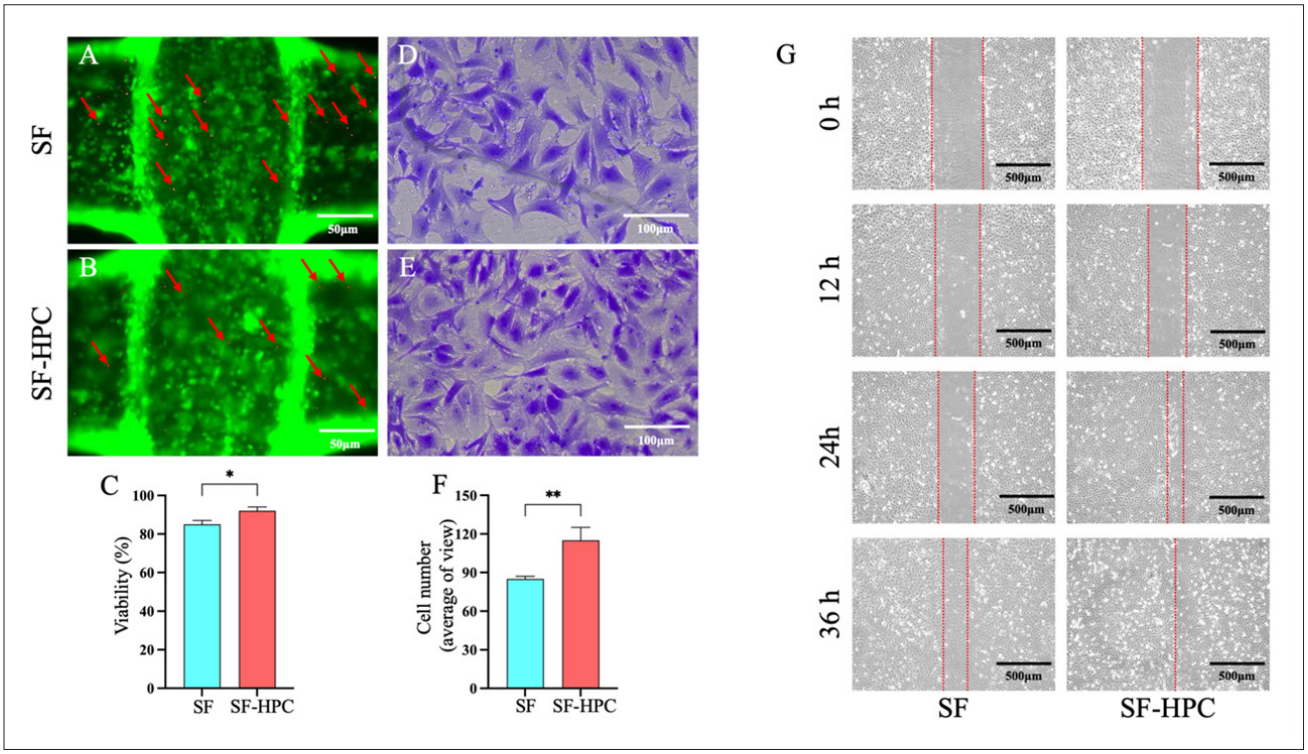

Figure 5. Cell viability and migration capacity in SF and SF–HPC tissue-engineered Achilles tendon scaffolds. (A, B) representative live/dead staining images of cells in SF and SF–HPC scaffolds after 72 h of culture. (C) Quantitative analysis of cell viability at 72 h. (D, E) Representative images of Transwell migration assay after 36 h. (F) Quantification of migrated cells per field in Transwell assays after 36 h. (G) Scratch assay images showing cell migration at 0, 12, 24, and 36 h. Scale bars: (A) 50 μm, (B) 50 μm, (D) 100 μm, (E) 100 μm, (G) 500 μm; magnifications: (A) 200×, (B) 200×, (D) 500×, (E) 500×, (G) 100×. $n = 3$; $^{*}p < 0.05$, $^{**}p < 0.01$. Abbreviations: HPC, hydroxypropyl cellulose; SF, silk fibroin.

groups (Figure 5G). The SF–HPC group demonstrated a narrower scratch gap and stronger cell migration capability compared to the SF group. Cell migration within scaffolds is critical for scaffold–host tissue integration.[55] Migratory cells infiltrate the defect site and fill the interface between the scaffold and host tissue, thereby promoting seamless integration.

To evaluate cell proliferation within the scaffolds, a CCK-8 assay was performed. The results showed gradual cell proliferation in both SF and SF–HPC scaffolds over time. At 12, 24, and 72 h, the SF–HPC group exhibited significantly higher proliferative activity compared to the SF group (Figure 6A). Cell proliferation is a pivotal factor in determining scaffold functionality and regenerative efficiency.[56] Proliferatively active TSPCs rapidly colonize the scaffold surface, migrate to the defect site, and secrete extracellular matrix components such as collagen, thereby forming a structural framework for neo-tendon tissue and accelerating Achilles tendon repair.

To assess the tenogenic differentiation capacity of TSPCs within the scaffolds, SF and SF–HPC scaffolds seeded with TSPCs were cultured *in vitro* and analyzed by PCR at weeks 2 and 4. The results demonstrated that the expression of the tenogenic marker *Scx* in the SF–HPC group was significantly higher than in the SF group at both time points. Conversely, the expression levels of chondrogenic (*Sox9*) and osteogenic (*Bmp2*) markers were significantly lower in the SF–HPC group compared to the SF group (Figure 6B–D). These findings indicate that SF–HPC scaffolds preferentially promote tenogenic differentiation of TSPCs.

The tenogenic differentiation capacity of TSPCs is a central driver of functional tissue regeneration. Tenogenically differentiated TSPCs mature into tenocytes, which directly synthesize and assemble type I collagen fibers—the critical structural component responsible for the mechanical strength of Achilles tendons.[57] Tenocyte activity governs collagen fiber alignment, density, and crosslinking, thereby determining the structural integrity of regenerated tendon tissue.[58]

In the pathological progression of HO following Achilles tendon injury, SOX-9 and BMP2 are key molecular drivers of aberrant bone formation.[59] SOX-9, a master transcriptional regulator of chondrogenesis,

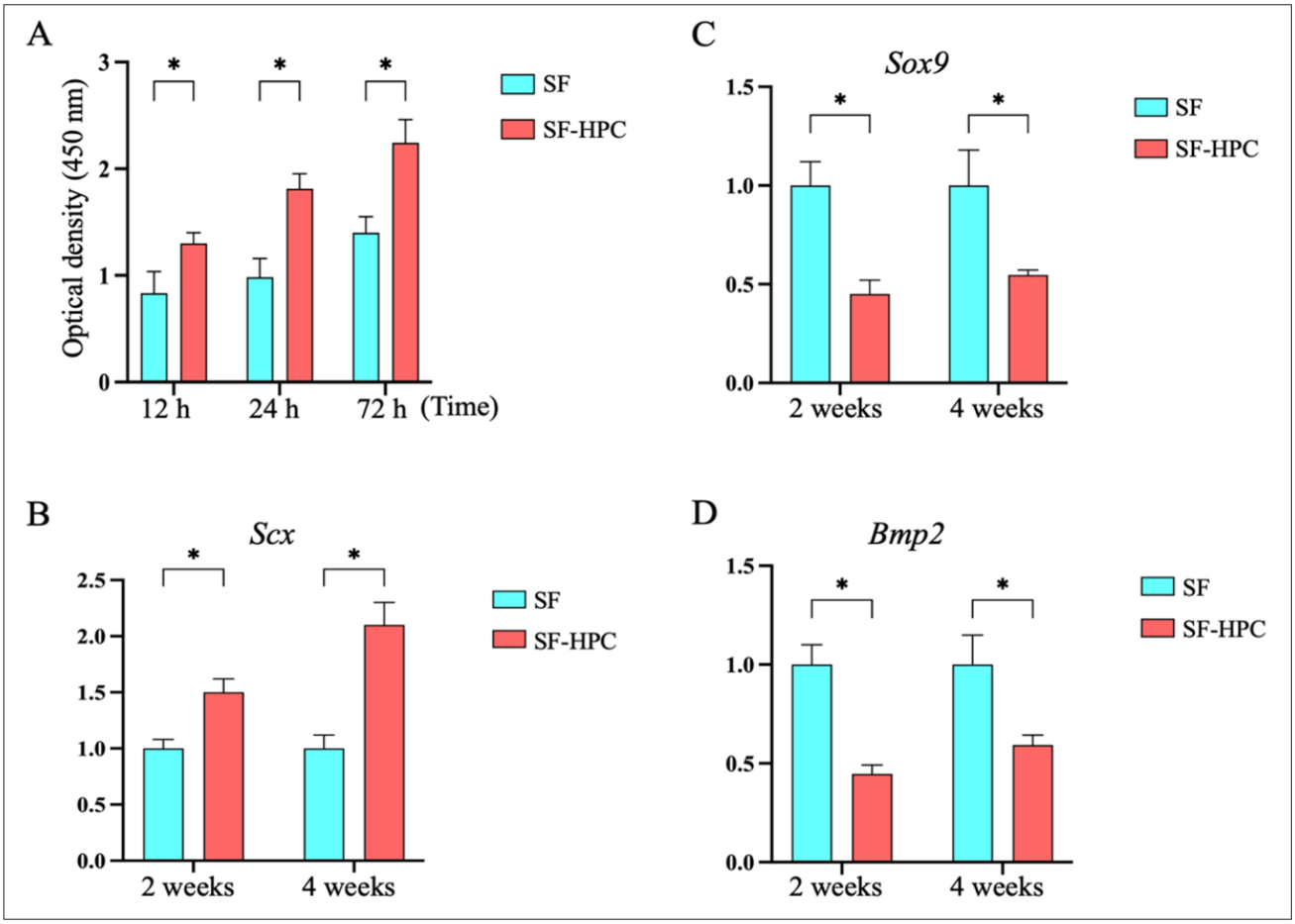

Figure 6. Proliferation and differentiation capacities of TSPCs in SF and SF–HPC tissue-engineered Achilles tendon scaffolds. (A) Proliferation analysis of TSPCs using the Cell Counting Kit-8 assay. (B–D) Quantitative polymerase chain reaction analysis of lineage-specific gene expression (*Scx*: tenogenic marker; *Sox9*: chondrogenic marker; *Bmp2*; osteogenic marker). $n = 3$; $^*p < 0.05$. Abbreviations: *Bmp2*, bone morphogenetic protein 2; HPC, hydroxypropyl cellulose; *Scx*, scleraxis; SF, silk fibroin; *Sox9*, SRY-box transcription factor; TSPCs, tendon stem/progenitor cells.

controls the expression of type II collagen and aggrecan. Downregulation of *Sox9* suppresses chondrogenic differentiation of TSPCs, eliminating the cartilage template required for endochondral ossification and thereby preventing HO initiation at its source. BMP2 activates osteogenic gene programs via the Smad1/5/8 signaling pathway, driving stem cell differentiation into osteoblasts and subsequent bone matrix deposition.[60] Reduced *Bmp2* expression directly disrupts this cascade, effectively minimizing HO and preventing tendon calcification or joint mobility impairment.

Within tissue-engineered Achilles tendon scaffolds, cellular viability, migration, proliferation, and differentiation collectively form a dynamic synergistic network that drives functional tissue regeneration.[61] Cell viability is the prerequisite for all subsequent cellular activities—high viability ensures the safety and biocompatibility of biomaterials while providing viable cellular resources for migration and proliferation. Cell migration orchestrates the directional distribution of cells toward the defect site, facilitating scaffold–host tissue interfacial integration and simultaneously creating pathways for vascularization and innervation. Cell proliferation replenishes cellular populations to fully cover the injury area, preventing delayed repair. The terminal differentiation of TSPCs into tenocytes marks the culmination of tendon regeneration, wherein tenocytes restore tendon mechanical properties through the secretion of aligned collagen fibers.

3.6. *In vivo* study on tissue-engineered Achilles tendon scaffolds for the prevention of post-traumatic heterotopic ossification

To evaluate the efficacy of tissue-engineered Achilles tendon scaffolds in preventing HO following tendon injury, an *in vivo* rat study was conducted. Achilles tendon injury

models were established via mid-tendon transection in rats (Figure 7E). Following transection, rats in the control group received no intervention beyond layered closure of fascia and skin. Rats implanted with SF scaffolds at the injury site were designated as the SF group, while those receiving SF–HPC scaffolds comprised the SF–HPC group. At 2, 4, and 8 weeks post-operatively, micro-CT scans were performed on all groups to quantify HO volume at the injury site. At 8 weeks, the skin and subcutaneous fascia overlying the Achilles tendon were surgically exposed for gross morphological evaluation. Tendon specimens were subsequently harvested for histological analyses, including H&E staining, Safranin O staining, and IHC staining.

Micro-CT results revealed no significant HO tissue at the Achilles tendon site in any group at 2 weeks post-operatively (Figure 7A1–C1). By 4 weeks, HO tissue volumes of approximately 2.1 mm^3, 1.7 mm^3, and 0.2 mm^3 were observed in the control, SF, and SF–HPC groups, respectively. The SF–HPC group exhibited a significantly smaller HO volume compared to both the control and SF groups (Figure 7A2–C2, D). At 8 weeks post-operatively, HO volumes increased to approximately 4.6 mm^3 in the control group and 2.4 mm^3 in the SF group, whereas the SF–HPC group maintained minimal HO (0.5 mm^3). The SF–HPC group consistently demonstrated significantly reduced HO volume compared to the other two groups at this time point (Figure 7A3–C3, D).

Gross examination and histological staining of rat Achilles tendons at 8 weeks post-operatively revealed that, in the control group, evident HO tissue was present at both the proximal and distal insertion sites of the tendon, accompanied by inflammatory hyperplasia and scar tissue formation (Figure 7A4). The SF group exhibited minimal HO tissue at the insertion sites, with sporadic scar tissue and irregular tendon morphology (Figure 7B4). In contrast, the SF–HPC group displayed no grossly visible HO tissue,

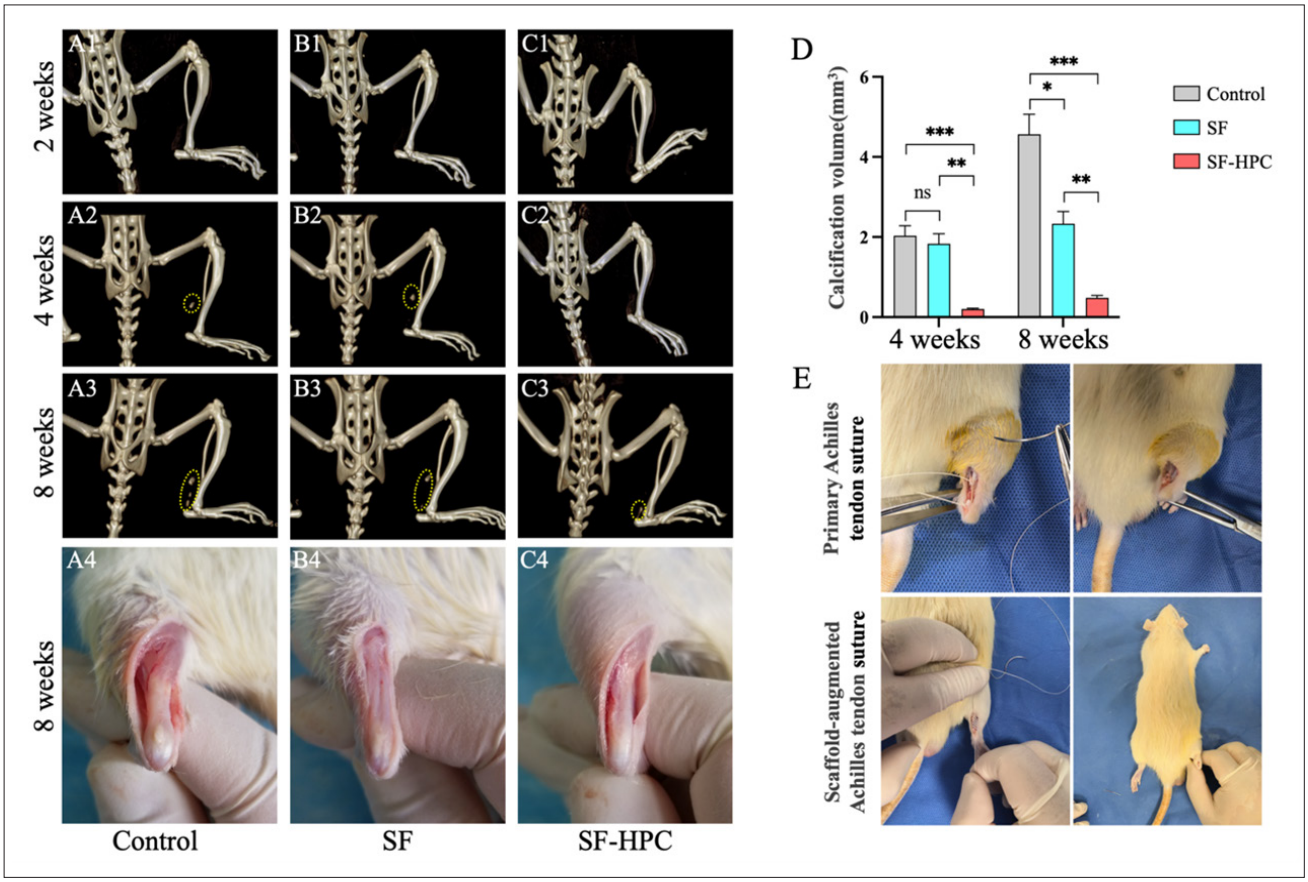

Figure 7. Evaluation of heterotopic ossification in rat models. (A1–A4) Micro-computed tomography reconstruction images of hindlimbs at 2, 4, and 8 weeks post-tenotomy, and gross morphology of regenerated tendons at 8 weeks in the control group. (B1–B4) Corresponding images for the SF group. (C1–C4) Corresponding images for the SF–HPC group. (D) Quantification of calcified tissue volume in Achilles tendons at 4 and 8 weeks post-operation. (E) Representative intraoperative photographs of primary suture versus scaffold-augmented suture in rat Achilles tendon. $n = 3$; $^*p < 0.05$, $^{**}p < 0.01$, $^{***}p < 0.001$. *Note*: Yellow dashed circles indicate regions of heterotopic ossification. Abbreviations: HPC, hydroxypropyl cellulose; SF, silk fibroin.

no significant inflammatory hyperplasia or scar tissue, and preserved tendon morphology (Figure 7C4).

Histological evaluation via H&E staining demonstrated extensive ossified tissue within the Achilles tendons of the control group, moderate ossification in the SF group, and minimal ossification in the SF–HPC group (Figure 8A1, B1, and C1). Safranin O staining corroborated these findings, showing similar spatial patterns of pathological matrix distribution (Figure 8A2, B2, and C2). IHC staining revealed widespread BMP-2-positive regions in the control group, localized BMP2 expression in the SF group, and only sporadic BMP2 signals in the SF–HPC group (Figure 8A3, B3, and C3). Quantitative IHC analysis confirmed a significantly reduced BMP-2-positive area in the SF–HPC group compared to both control and SF groups (Figure 8D).

In assessing the *in vivo* efficacy of tissue-engineered scaffolds for preventing post-traumatic HO, micro-CT, H&E staining, Safranin O staining, and IHC staining served as complementary and indispensable analytical modalities. Together, these techniques provided multi-dimensional insights into tissue quantification (micro-CT), histoarchitecture (HE), matrix composition (Safranin O), and molecular signaling (IHC), establishing a robust framework for evaluating therapeutic outcomes.[62–65]

3.7. Evaluation of systemic inflammatory and immune responses following implantation of tissue-engineered Achilles tendon scaffolds

To assess systemic inflammatory and immune responses after scaffold implantation, venous blood was collected from rats at 3, 7, and 14 days post-operatively following Achilles tendon transection. The measured parameters included WBC count, red blood cell count, neutrophil count, neutrophil percentage, lymphocyte count, lymphocyte percentage, monocyte count, and monocyte percentage.

The WBC count results demonstrated a gradual decrease over time across all groups. Notably, the control group exhibited a significant acute inflammatory response at post-operative day 3, while the SF–HPC group showed lower WBC counts compared to both the Control and SF groups (Figure 9A). These findings indicate that scaffold implantation did not induce marked systemic inflammatory reactions.

Red blood cell counts increased progressively in all groups. However, the control group displayed a significant

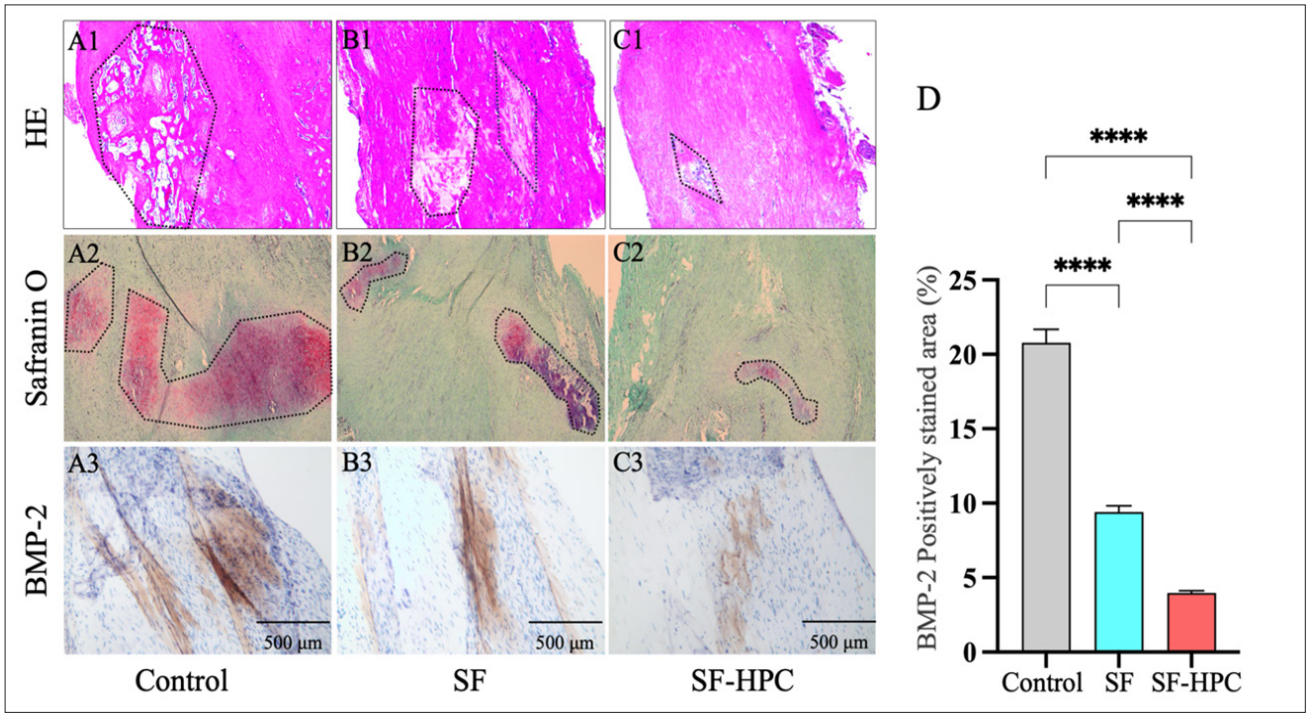

Figure 8. Histopathological and molecular characterization of regenerated Achilles tendons at eight weeks post-tenotomy. (A1, B1, C1) Representative hematoxylin and eosin (HE) staining of tendon tissues in control, SF, and SF–HPC groups. (A2, B2, C2) Safranin O staining for proteoglycan deposition. (A3, B3, C3) Immunohistochemical staining of BMP-2 expression. Scale bar: 500 μm; magnification: 100×. (D) Quantification of BMP-2 positively stained areas in immunohistochemical analysis. $n = 3$; ****$p < 0.0001$. *Note*: Black dashed boxes demarcate calcified regions. Abbreviations: BMP-2, bone morphogenetic protein 2; HPC, hydroxypropyl cellulose; SF, silk fibroin.

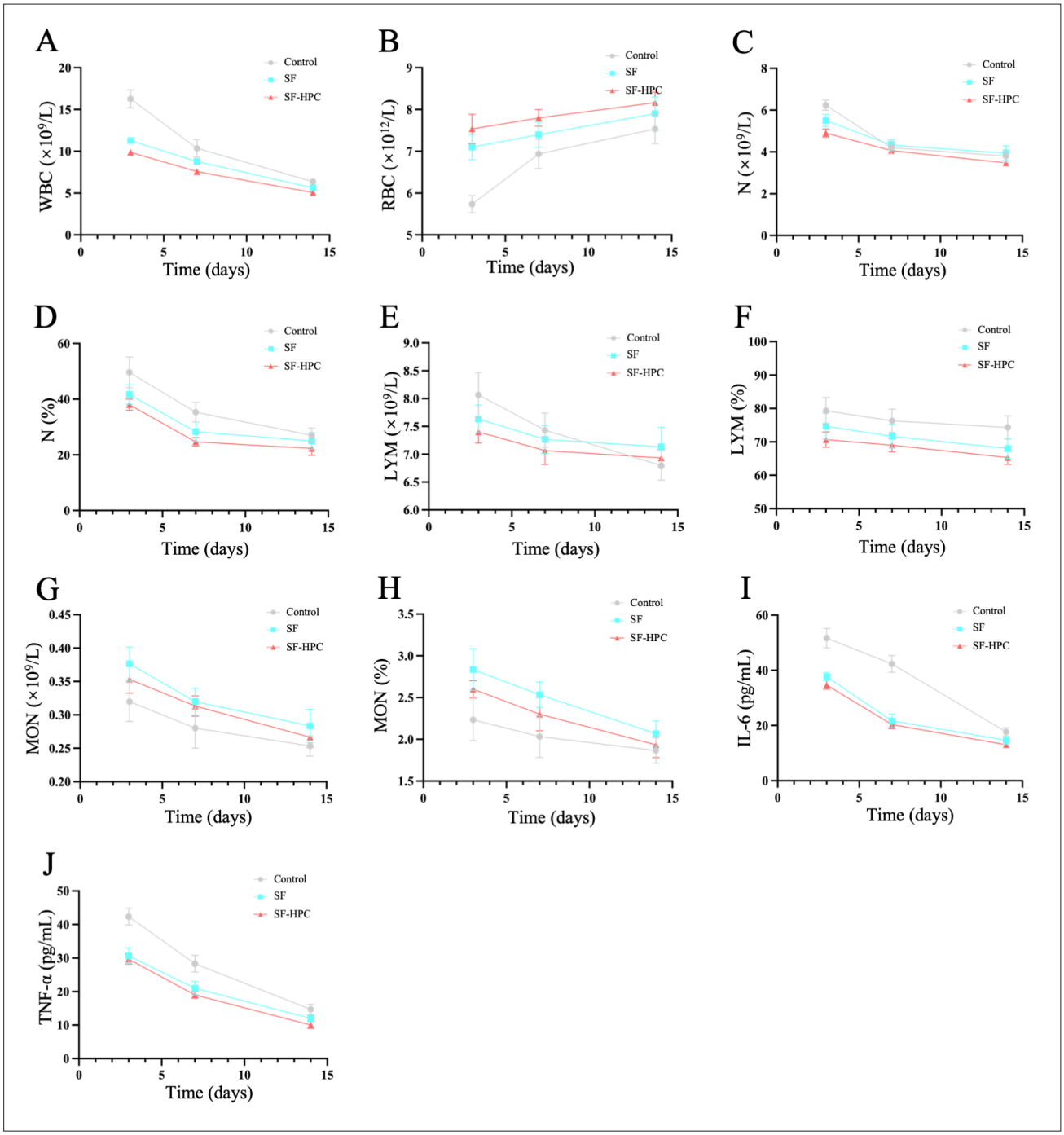

Figure 9. Systemic inflammatory profiles in rat models after Achilles tenotomy. (A) WBC count. (B) RBC count. (C) Neutrophil (N) count. (D) Neutrophil (N) percentage. (E) LYM count. (F) LYM percentage. (G) MON count. (H) MON percentage. (I) IL-6 concentration. (J) TNF-α concentration. $n = 3$; $^{*}p < 0.05$, $^{**}p < 0.01$, $^{***}p < 0.001$. Abbreviations: HPC, hydroxypropyl cellulose; SF, silk fibroin; LYM, lymphocyte; RBC, red blood cell; WBC, white blood cell; MON, monocyte; IL-6, interleukin-6; TNF-α, tumor necrosis factor-α.

reduction in red blood cell count at post-operative day 3, suggesting substantial hemorrhage and erythrocyte loss during the early post-operative phase (Figure 9B).

Neutrophil counts and percentages gradually returned to baseline levels in all groups. The control group showed abnormally elevated neutrophil counts and percentages at day 3, exceeding normal physiological ranges, whereas the SF and SF–HPC groups maintained neutrophil parameters within normal limits (Figure 9C and D). These results further confirm the absence of acute inflammatory responses following scaffold implantation.

Lymphocyte counts and percentages normalized progressively across all groups, with no significant intergroup differences observed (Figure 9E and F). This pattern indicates that tendon transection surgery alone did not elicit chronic inflammatory responses, regardless of the intervention.

Similarly, monocyte counts and percentages returned to baseline levels across all groups over the observation period (Figure 9G and H). Collectively, these hematological profiles demonstrate that neither scaffold implantation nor surgical injury provoked detectable immune dysregulation.

Additionally, serum levels of pro-inflammatory cytokines (IL-6 and TNF-α) were quantified at post-operative days 3, 7, and 14. IL-6 levels in the control group significantly surged at post-operative day 3, exceeding those in both the SF and SF–HPC groups ($p < 0.05$). By post-operative day 14, IL-6 levels in the control group returned to baseline. In contrast, no statistically significant difference was observed between the SF and SF–HPC groups, both of which exhibited a gradual decline in IL-6 concentrations, returning to near-baseline levels by post-operative day 7 and fully normalizing by post-operative day 14 (Figure 9I). A similar trend was observed for TNF-α (Figure 9J). Collectively, these findings indicate that neither SF nor SF–HPC scaffolds induced sustained elevation of inflammatory cytokines post-implantation, with cytokine levels largely restored within 1–2 weeks.

SF intrinsically possesses immunomodulatory properties. As demonstrated in previous research, SF-based materials attenuate pro-inflammatory cytokine secretion (e.g., TNF-α, IL-6) through suppression of inflammatory pathways such as nuclear factor kappa-light-chain-enhancer of activated B cell signaling.[66] This reduction in pro-inflammatory cytokines directly impairs neutrophil and monocyte recruitment, thereby decreasing WBC infiltration into inflammatory sites—a phenomenon reflected by diminished peripheral blood WBC counts.[67]

In the prevention of post-traumatic HO by tissue-engineered Achilles tendon scaffolds, attenuated inflammatory and immune responses play a critical role in regulating key pathological mechanisms.[13] Pro-inflammatory cytokines upregulate BMP-2 and Wnt signaling pathways, driving stem cell differentiation toward osteoblasts.[68] Suppression of inflammatory responses directly inhibits these pathways, thereby reducing ectopic bone matrix deposition.

Neutrophil-derived reactive oxygen species and matrix metalloproteinases (MMPs) disrupt the local microenvironment, promoting calcium salt deposition. A hypoimmune response inhibits immune cell-mediated aberrant repair processes.[69,70] A low-inflammatory microenvironment downregulates BMP-2/Smad1/5 signaling while upregulating tenogenic markers such as *Scx*, directing stem cell differentiation toward tenocytes rather than osteoblasts. Concurrently, reduced MMP activity preserves type I collagen integrity by minimizing its degradation, maintaining ordered collagen fiber alignment, and enhancing mechanical stability.[70–72]

In summary, reduced inflammatory and immune responses play a crucial role in preventing HO of the Achilles tendon by suppressing osteogenic signaling, optimizing stem cell differentiation, and blocking aberrant repair processes.

Collectively, the SF–HPC scaffold demonstrates exceptional mechanical properties, tunable degradation kinetics, and favorable biocompatibility, enabling effective tendon repair while preventing HO. Compared to collagen scaffolds, SF-based scaffolds provide superior degradation resistance and mechanical strength. Although collagen offers excellent biocompatibility, its low mechanical integrity and rapid degradation may lead to premature loss of structural support post-implantation. In contrast, appropriately cross-linked SF scaffolds maintain biocompatibility while enhancing mechanical robustness and controlling degradation rates, thereby providing sustained tissue support.[73] A distinct advantage over PLGA scaffolds lies in SF's ability to better facilitate cell adhesion and proliferation,[74] a finding corroborated by our experimental results.

4. Conclusion

This study successfully formulated an SF–HPC–TSPC bioink, utilizing SF as the base material, HPC as a reinforcing agent, and TSPCs as seed cells. The developed bioink exhibited excellent cytocompatibility and favorable rheological properties. It enabled 3D bioprinting of porous tissue-engineered Achilles tendon scaffolds with high mechanical strength and controlled

biodegradability, achieving an elastic modulus of 85 MPa and a porosity of 91%. *In vitro* studies demonstrated that SF–HPC scaffolds significantly enhanced TSPCs viability, migration, proliferation, and tenogenic differentiation. *In vivo* evaluations confirmed the scaffolds' superior biocompatibility, as they elicited no detectable systemic inflammatory or immune responses. Importantly, the SF–HPC scaffolds effectively prevented HO in our rat Achilles tendon injury model.

Acknowledgments

None.

Funding

This work was supported by the National Major Research Plan of the National Natural Science Foundation of China (NSFC) (92368201), the National Key Research and Development Project (2021YFA1201404), the Major Project of NSFC (81991514), and the Jiangsu Province Medical Innovation Center of Orthopedic Surgery (CXZX202214).

Conflict of interest

The authors declare that they have no competing interests.

Author contributions

Conceptualization: Kai Yan, Xianzong Ning
Formal analysis: Minghao Zhang, Yutao Yang
Funding acquisition: Xianzong Ning, Kai Yan
Investigation: Xianzong Ning, Kai Yan, Rui Du
Methodology: Kai Yan, Rui Du
Visualization: Kai Yan, Xiaoming Xu, Baoyuan Meng
Writing–original draft: Kai Yan, Rui Du
Writing–review & editing: Kai Yan, Fei Yu

Ethics approval and consent to participate

All animal experiments in this study were conducted in accordance with standard procedures and approved by the Ethics Committee of Nanjing Drum Tower Hospital Affiliated with Nanjing University Medical School (Approval No.: 2021AE01031).

Consent for publication

Not applicable.

Availability of data

The data supporting the findings of this study are available on request from the corresponding author upon reasonable request.

References

1. Traweger A, Scott A, Kjaer M, et al. Achilles tendinopathy. *Nat Rev Dis Primers*. 2025;11(1):20.
doi: 10.1038/s41572-025-00602-9

2. Fischer S. Acute rupture of the Achilles tendon: diagnostics, treatment and aftercare. *Unfallchirurgie (Heidelb)*. 2024;127(8):597-606.
doi: 10.1007/s00113-024-01454-w

3. Geuskens W, Caekebeke P, VAN Riet R. Prevalence and clinical implications of heterotopic ossification after distal biceps tendon repair. *Acta Orthop Belg*. 2023;89(4):695-700.
doi: 10.52628/89.4.12447

4. Fischer CS, Porsche J, Leyder D, Schüll D, Histing T, Ziegler P. Heterotopic ossification following severe radial head fractures: clinical outcome and associated factors. *Jt Dis Relat Surg*. 2025;36(1):47-55.
doi: 10.52312/jdrs.2025.1992

5. Dai G, Li Y, Liu J, et al. Higher BMP Expression in tendon stem/progenitor cells contributes to the increased heterotopic ossification in achilles tendon with aging. *Front Cell Dev Biol*. 2020;8:570605.
doi: 10.3389/fcell.2020.570605

6. Yu T, Zhang J, Zhu W, et al. Chondrogenesis mediates progression of ankylosing spondylitis through heterotopic ossification. *Bone Res*. 2021;9(1):19.
doi: 10.1038/s41413-021-00140-6

7. Wang Z, Yi X, Liu Y, Liu Q, Li Z, Yu A. Differential expression profiles and functional prediction of circRNA in mice with traumatic heterotopic ossification. *Front Immunol*. 2022;13:1090529.
doi: 10.3389/fimmu.2022.1090529

8. Xu L, Xu K, Wu Z, et al. Pioglitazone attenuates advanced glycation end products-induced apoptosis and calcification by modulating autophagy in tendon-derived stem cells. *J Cell Mol Med*. 2020;24(3):2240-2251.
doi: 10.1111/jcmm.14901

9. Tachibana N, Chijimatsu R, Okada H, et al. RSPO2 defines a distinct undifferentiated progenitor in the tendon/ligament and suppresses ectopic ossification. *Sci Adv*. 2022;8(33):eabn2138.
doi: 10.1126/sciadv.abn2138

10. Wang T, Chen P, Chen L, et al. Reduction of mechanical loading in tendons induces heterotopic ossification and activation of the β-catenin signaling pathway. *J Orthop Transl*. 2021;29:42-50.
doi: 10.1016/j.jot.2021.03.004

11. Pierantoni M, Hammerman M, Silva Barreto I, et al. Spatiotemporal and microstructural characterization of heterotopic ossification in healing rat Achilles tendons. *FASEB J*. 2023;37(6).
doi: 10.1096/fj.202201018RRR

12. Yamaguchi H, Li M, Kitami M, Swaminathan S, Mishina Y, Komatsu Y. Enhanced BMP signaling in Cathepsin K-positive tendon progenitors induces heterotopic ossification. *Biochem Biophys Res Commun*. 2023;688:149147. doi: 10.1016/j.bbrc.2023.149147

13. Magnusson SP, Agergaard AS, Couppé C, et al. Heterotopic ossification after an achilles tendon rupture cannot be prevented by early functional rehabilitation: a cohort study. *Clin Orthop Relat Res*. 2020;478(5):1101-1108. doi: 10.1097/corr.0000000000001085

14. Agarwal S, Loder S, Levi B. Heterotopic ossification following upper extremity injury. *Hand Clin*. 2017;33(2): 363-373. doi: 10.1016/j.hcl.2016.12.013

15. Delgado Caceres M, Angerpointner K, Galler M, et al. Tenomodulin knockout mice exhibit worse late healing outcomes with augmented trauma-induced heterotopic ossification of Achilles tendon. *Cell Death Dis*. 2021;12(11):1049. doi: 10.1038/s41419-021-04298-z

16. Walden G, Liao X, Donell S, Raxworthy MJ, Riley GP, Saeed A. A clinical, biological, and biomaterials perspective into tendon injuries and regeneration. *Tissue Eng Part B Rev*. 2017;23(1):44-58. doi: 10.1089/ten.TEB.2016.0181

17. No YJ, Castilho M, Ramaswamy Y, Zreiqat H. Role of biomaterials and controlled architecture on tendon/ligament repair and regeneration. *Adv Mater*. 2020;32(18):e1904511. doi: 10.1002/adma.201904511

18. Sensini A, Cristofolini L. Biofabrication of electrospun scaffolds for the regeneration of tendons and ligaments. *Materials (Basel)*. 2018;11(10):1963. doi: 10.3390/ma11101963

19. Yan K, Zhang X, Liu Y, et al. 3D-bioprinted silk fibroin-hydroxypropyl cellulose methacrylate porous scaffold with optimized performance for repairing articular cartilage defects. *Mater Des*. 2023;225:111531. doi: 10.1016/j.matdes.2022.111531

20. Zhang X, Liu Y, Zuo Q, et al. 3D bioprinting of biomimetic bilayered scaffold consisting of decellularized extracellular matrix and silk fibroin for osteochondral repair. *Int J Bioprint*. 2021;7(4):401. doi: 10.18063/ijb.v7i4.401

21. Park W, Gao G, Cho DW. Tissue-specific decellularized extracellular matrix bioinks for musculoskeletal tissue regeneration and modeling using 3d bioprinting technology. *Int J Mol Sci*. 2021;22(15):7837. doi: 10.3390/ijms22157837

22. Jiu J, Liu H, Li D, et al. 3D bioprinting approaches for spinal cord injury repair. *Biofabrication*. 2024;16(3). doi: 10.1088/1758-5090/ad3a13

23. Zhang Y, Sun Y, Luo J, et al. Hydrogel-based materials for mandibular reconstruction. *MSAM*. 2025;4(2). doi: 10.36922/msam025070006

24. Li H, Zeng S, Zhou L. Biocompatible nanogels with tunable size and tailorable properties: a simple synthesis by self-assembly and disulfide crosslinking of amphiphilic hyperbranched peach gum polysaccharide. *Int J Biol Macromol*. 2025;309(Pt 4):143083. doi: 10.1016/j.ijbiomac.2025.143083

25. Zhang DKY, Brockman JM, Adu-Berchie K, et al. Subcutaneous biodegradable scaffolds for restimulating the antitumour activity of pre-administered CAR-T cells. *Nat Biomed Eng*. 2025;9(2):268-278. doi: 10.1038/s41551-024-01216-4

26. Xu Y, Huang J, Mai Y, et al. CBD-conjugated BMP-inhibiting exosomes on collagen scaffold dual-target Achilles tendon repair: synergistic regeneration and heterotopic ossification prevention. *Mater Today Bio*. 2025;32:101790. doi: 10.1016/j.mtbio.2025.101790

27. Avenoso A, Bruschetta G, D'Ascola A, et al. Hyaluronan fragments produced during tissue injury: A signal amplifying the inflammatory response. *Arch Biochem Biophys*. 2019;663:228-238. doi: 10.1016/j.abb.2019.01.015

28. Kim JK, Go EJ, Ko KW, et al. PLGA microspheres containing hydrophobically modified magnesium hydroxide particles for acid neutralization-mediated anti-inflammation. *Tissue Eng Regen Med*. 2021;18(4):613-622. doi: 10.1007/s13770-021-00338-z

29. Wang Y, Feng X, Chen X. Autonomous bioelectronic devices based on silk fibroin. *Adv Mater*. 2025;37(22):e2500073. doi: 10.1002/adma.202500073

30. Shen C, Zhou Z, Li R, et al. Silk fibroin-based hydrogels for cartilage organoids in osteoarthritis treatment. *Theranostics*. 2025;15(2):560-584. doi: 10.7150/thno.103491

31. Wang F, Lei H, Tian C, et al. An efficient biosynthetic system for developing functional silk fibroin-based biomaterials. *Adv Mater*. 2025;37(7):e2414878. doi: 10.1002/adma.202414878

32. Cai G, Zhao W, Zhu T, Oliveira AL, Yao X, Zhang Y. Effects of protein conformational transition accompanied with crosslinking density cues in silk fibroin hydrogels on the proliferation and chondrogenesis of encapsulated stem cells. *Regen Biomater*. 2025;12:rbaf019. doi: 10.1093/rb/rbaf019

33. Ben X, Lu X, Zhao G, Wei Z, Yang J, Kan Y. Internal secondary structural conformational states of silk fibroin studied by raman spectroscopy with band deconvolution analysis. *Biomacromolecules*. 2025;26(3):1992-2002. doi: 10.1021/acs.biomac.4c01827

34. Ji X, Li Y, Wang J, et al. Silk protein gene engineering and its applications: recent advances in biomedicine driven by molecular biotechnology. *Drug Des Devel Ther*. 2025;19:599-626.
doi: 10.2147/dddt.S504783

35. Yin J, Fang Y, Xu L, Ahmed A. High-throughput fabrication of silk fibroin/hydroxypropyl methylcellulose (SF/HPMC) nanofibrous scaffolds for skin tissue engineering. *Int J Biol Macromol*. 2021;183:1210-1221.
doi: 10.1016/j.ijbiomac.2021.05.026

36. Su D, Yao M, Liu J, Zhong Y, Chen X, Shao Z. Enhancing mechanical properties of silk fibroin hydrogel through restricting the growth of β-sheet domains. *ACS Appl Mater Interfaces*. 2017;9(20):17489-17498.
doi: 10.1021/acsami.7b04623

37. Bi Y, Ehirchiou D, Kilts TM, et al. Identification of tendon stem/progenitor cells and the role of the extracellular matrix in their niche. *Nat Med*. 2007;13(10):1219-1227.
doi: 10.1038/nm1630

38. He W, Jiang C, Zhou P, Hu X, Gu X, Zhang S. Role of tendon-derived stem cells in tendon and ligament repair: focus on tissue engineer. *Front Bioeng Biotechnol*. 2024;12:1357696.
doi: 10.3389/fbioe.2024.1357696

39. Chen J, Jiang C, Yin L, et al. A review of the role of tendon stem cells in tendon-bone regeneration. *Med Sci Monit*. 2023;29:e940805.
doi: 10.12659/msm.940805

40. Lu J, Chen H, Lyu K, et al. The functions and mechanisms of tendon stem/progenitor cells in tendon healing. *Stem Cells Int*. 2023;2023:1258024.
doi: 10.1155/2023/1258024

41. Jahani A, Nourbakhsh MS, Ebrahimzadeh MH, Mohammadi M, Yari D, Moradi A. Biomolecules-loading of 3D-printed alginate-based scaffolds for cartilage tissue engineering applications: a review on current status and future prospective. *Arch Bone Jt Surg*. 2024;12(2):92-101.
doi: 10.22038/abjs.2023.73275.3396

42. Li M, Shi T, Yao D, Yue X, Wang H, Liu K. High-cytocompatible semi-IPN bio-ink with wide molecular weight distribution for extrusion 3D bioprinting. *Sci Rep*. 2022;12(1):6349.
doi: 10.1038/s41598-022-10338-1

43. Delkash Y, Gouin M, Rimbeault T, et al. Bioprinting and in vitro characterization of an eggwhite-based cell-laden patch for endothelialized tissue engineering applications. *J Funct Biomater*. 2021;12(3):45.
doi: 10.3390/jfb12030045

44. Kolluru PV, Lipner J, Liu W, et al. Strong and tough mineralized PLGA nanofibers for tendon-to-bone scaffolds. *Acta Biomater*. 2013;9(12):9442-9450.
doi: 10.1016/j.actbio.2013.07.042

45. Jacob S, Reshmy R, Antony S, et al. Nanocellulose in tissue engineering and bioremediation: mechanism of action. *Bioengineered*. 2022;13(5):12823-12833.
doi: 10.1080/21655979.2022.2074739

46. Veronesi F, Giavaresi G, Bellini D, Casagranda V, Pressato D, Fini M. Evaluation of a new collagen-based medical device (ElastiCo®) for the treatment of acute Achilles tendon injury and prevention of peritendinous adhesions: An in vitro biocompatibility and in vivo investigation. *J Tissue Eng Regen Med*. 2020;14(8):1113-1125.
doi: 10.1002/term.3085

47. Webb WR, Dale TP, Lomas AJ, et al. The application of poly(3-hydroxybutyrate-co-3-hydroxyhexanoate) scaffolds for tendon repair in the rat model. *Biomaterials*. 2013;34(28):6683-6694.
doi: 10.1016/j.biomaterials.2013.05.041

48. Kim SH, Park JH, Kwon JS, et al. NIR fluorescence for monitoring in vivo scaffold degradation along with stem cell tracking in bone tissue engineering. *Biomaterials*. 2020;258:120267.
doi: 10.1016/j.biomaterials.2020.120267

49. Salehi S, Koeck K, Scheibel T. Spider silk for tissue engineering applications. *Molecules*. 2020;25(3):737.
doi: 10.3390/molecules25030737

50. Xie Y, Zhang F, Akkus O, King MW. A collagen/PLA hybrid scaffold supports tendon-derived cell growth for tendon repair and regeneration. *J Biomed Mater Res B Appl Biomater*. 2022;110(12):2624-2635.
doi: 10.1002/jbm.b.35116

51. Shirosaki Y, Tsukatani Y, Okamoto K, Hayakawa S, Osaka A. Preparation and drug release profile of chitosan-siloxane hybrid capsules coated with hydroxyapatite. *Pharmaceutics*. 2022;14(5):1111.
doi: 10.3390/pharmaceutics14051111

52. Fei Y, Ma Y, Zhang H, Li H, Feng G, Fang J. Nanotechnology for research and treatment of the intestine. *J Nanobiotechnol*. 2022;20(1):430.
doi: 10.1186/s12951-022-01517-3

53. Sadeghzadeh H, Mehdipour A, Dianat-Moghadam H, et al. PCL/Col I-based magnetic nanocomposite scaffold provides an osteoinductive environment for ADSCs in osteogenic cues-free media conditions. *Stem Cell Res Ther*. 2022;13(1):143.
doi: 10.1186/s13287-022-02816-0

54. Zheng A, Wang X, Xin X, et al. Promoting lacunar bone regeneration with an injectable hydrogel adaptive to the microenvironment. *Bioact Mater*. 2023;21:403-421.
doi: 10.1016/j.bioactmat.2022.08.031

55. Eggermont LJ, Rogers ZJ, Colombani T, Memic A, Bencherif SA. Injectable cryogels for biomedical applications. *Trends Biotechnol*. 2020;38(4):418-431.
doi: 10.1016/j.tibtech.2019.09.008

56. Yao X, Yang Y, Zhou Z. Non-mulberry silk fiber-based composite scaffolds containing millichannels for auricular cartilage regeneration. *ACS Omega*. 2022;7(17):15064-15073. doi: 10.1021/acsomega.2c00846

57. Wang Y, Jin S, Luo D, et al. Functional regeneration and repair of tendons using biomimetic scaffolds loaded with recombinant periostin. *Nat Commun*. 2021;12(1):1293. doi: 10.1038/s41467-021-21545-1

58. Markel DC, Dietz P, Provenzano G, Bou-Akl T, Ren WP. Attachment and growth of fibroblasts and tenocytes within a porous titanium scaffold: a bioreactor approach. *Arthroplast Today*. 2022;14:231-236.e1. doi: 10.1016/j.artd.2021.12.003

59. Lin L, Shen Q, Xue T, Yu C. Heterotopic ossification induced by Achilles tenotomy via endochondral bone formation: expression of bone and cartilage related genes. *Bone*. 2010;46(2):425-431. doi: 10.1016/j.bone.2009.08.057

60. Cai Z, Wu B, Ye G, et al. Enhanced osteogenic differentiation of human bone marrow mesenchymal stem cells in ossification of the posterior longitudinal ligament through activation of the BMP2-Smad1/5/8 pathway. *Stem Cells Dev*. 2020;29(24):1567-1576. doi: 10.1089/scd.2020.0117

61. Zhang H, Liu MF, Liu RC, Shen WL, Yin Z, Chen X. Physical microenvironment-based inducible scaffold for stem cell differentiation and tendon regeneration. *Tissue Eng Part B Rev*. 2018;24(6):443-453. doi: 10.1089/ten.TEB.2018.0018

62. Brownley RC, Agarwal S, Loder S, et al. Characterization of heterotopic ossification using radiographic imaging: evidence for a paradigm shift. *PLoS One*. 2015;10(11):e0141432. doi: 10.1371/journal.pone.0141432

63. Foley KL, Hebela N, Keenan MA, Pignolo RJ. Histopathology of periarticular non-hereditary heterotopic ossification. *Bone*. 2018;109:65-70. doi: 10.1016/j.bone.2017.12.006

64. Ng J, Wei Y, Zhou B, et al. Ectopic implantation of juvenile osteochondral tissues recapitulates endochondral ossification. *J Tissue Eng Regen Med*. 2018;12(2):468-478. doi: 10.1002/term.2500

65. Fujihara R, Chiba Y, Nakagawa T, et al. Histomorphometry of ectopic mineralization using undecalcified frozen bone sections. *Microsc Res Tech*. 2018;81(11):1318-1324. doi: 10.1002/jemt.23140

66. Yuan J, Sun W, Zhang Z, et al. 5-Fluorouracil/curcumin loaded silk fibroin hydrogel for the adjuvant therapy in colorectal cancer. *Biomater Adv*. 2025;168:214108. doi: 10.1016/j.bioadv.2024.214108

67. Yeo D, Hwang SJ, Song YS, Lee HJ. Humulene inhibits acute gastric mucosal injury by enhancing mucosal integrity. *Antioxidants (Basel)*. 2021;10(5):761. doi: 10.3390/antiox10050761

68. Jian J, Sun L, Cheng X, Hu X, Liang J, Chen Y. Calycosin-7-O-β-d-glucopyranoside stimulates osteoblast differentiation through regulating the BMP/WNT signaling pathways. *Acta Pharm Sin B*. 2015;5(5):454-460. doi: 10.1016/j.apsb.2015.06.005

69. Winterbourn CC, Kettle AJ, Hampton MB. Reactive oxygen species and neutrophil function. *Annu Rev Biochem*. 2016;85:765-792. doi: 10.1146/annurev-biochem-060815-014442

70. Hong SY, Jiang HC, Xu WC, Zeng HS, Wang SG, Qin BL. Bioinformatics analysis reveals the potential role of matrix metalloproteinases in immunity and urolithiasis. *Front Immunol*. 2023;14:1158379. doi: 10.3389/fimmu.2023.1158379

71. Lu P, Chen Z, Wu M, et al. Type I collagen extracellular matrix facilitates nerve regeneration via the construction of a favourable microenvironment. *Burns Trauma*. 2024;12:tkae049. doi: 10.1093/burnst/tkae049

72. Gong SQ, Tang L, Liu Z, et al. NDGA enhances the physicochemical and anti-biodegradation performance of dentin collagen. *Oral Dis*. 2023;29(8):3525-3539. doi: 10.1111/odi.14453

73. Georgopoulou A, Papadogiannis F, Batsali A, et al. Chitosan/gelatin scaffolds support bone regeneration. *J Mater Sci Mater Med*. 2018;29(5):59. doi: 10.1007/s10856-018-6064-2

74. Chachlioutaki K, Karavasili C, Adamoudi E, et al. Silk sericin/PLGA electrospun scaffolds with anti-inflammatory drug-eluting properties for periodontal tissue engineering. *Biomater Adv*. 2022;133:112723. doi: 10.1016/j.msec.2022.112723